University of Dayton
eCommons

Electrical and Computer Engineering Faculty Publications

Department of Electrical and Computer Engineering

Numerical Examination of Acousto-optic Bragg Interactions for Profiled Lightwaves Using a Transfer Function Formalism

Monish Ranjan Chatterjee
University of Dayton, mchatterjee1@udayton.edu

Fares S. Almehmadi
University of Dayton

Numerical examination of acousto-optic Bragg interactions for profiled lightwaves using a transfer function formalism

Monish R. Chatterjee[1*] and Fares S. Almehmadi[1]

[1]University of Dayton, Dept. of ECE, 300 College Park, Dayton, OH 45469-0232

*corresponding author

Email: mchatterjee1@udayton.edu

ABSTRACT

Classically, acousto-optic (AO) interactions comprise scattering of photons by energetic phonons into higher and lower orders. Standard weak interaction theory describes diffraction in the Bragg regime as the propagation of a *uniform* plane wave of light through a *uniform* plane wave of sound, resulting in the well-known first- and zeroth-order diffraction. Our preliminary investigation of the nature of wave diffraction and photon scattering from a Bragg cell under intensity feedback with *profiled* light beams indicates that the diffracted (upshifted photon) light continues to maintain the expected (*uniform* plane wave) behavior versus the optical phase shift in the cell within a small range of the Q-parameter, and at larger Qs, begins to deviate. Additionally, we observe the asymptotic axial shift of the beam center as predicted by the transfer function formalism.

Keywords: photon, phonon, profiled beams, transfer function, diffraction, Bragg, Klein-Cook parameter, optical phase-shift.

1. INTRODUCTION AND BACKGROUND

Acousto-optic (AO) diffraction of light has many useful applications in the area of signal processing, including laser beam deflection, modulation, filtering, and encryption/ decryption when used with feedback [1]. Although these devices are well characterized and studied, a full physical understanding of the interactions is still relatively incomplete, and most analyses rely on a series of assumptions (such as weak interactions, uniform plane waves, and so on). This highly complex wave-particle problem may simultaneously be described via Maxwell's equations, and also a quantum description whereby the upshifted and downshifted orders of diffracted light are represented by a *wave-vector triad* consisting of two photons and one phonon.

It is well known that there are two regimes of operation for such a device, determined by the Klein-Cook parameter $Q\left(=LK^2/k\right)$. In this equation, L is the effective length of acousto-optic modulator, k is the wave number of light in the medium, and K is the wave number of sound [2]. Chatterjee and Chen [3] showed that for strict Bragg operation, Q should be larger than 8π. In this case, if the incident angle is at the Bragg angle $\theta_B\left(\approx K/2k\right)$, then there is only one diffracted order along with the zeroth or non-diffracted order. This is the most common mode of operation for AO modulators [4].

For Q much less than one, as controlled by the thickness L, and an incident beam that is approximately normal to the acoustic beam, the mode of operation is called the Raman-Nath regime. This is also called the thin grating regime because $L\left(<<\Lambda^2/\lambda\right)$, where Λ is the acoustic wavelength and λ is the incident light wavelength. This is characterized by multiple diffracted orders whose intensities are given by first- order Bessel functions [2, 5].

The traditional AO chaos problem, which stimulated this work, is studied under the assumption of a uniform plane wave input. Under this assumption, the usual *monostable, bistable* and *multistable* behavior are observed, leading to chaotic behavior under certain limits [6]. In reality, however, the incoming light wave is almost always non-uniform. Because of this, it is necessary to consider the propagation of non-uniform profiles through the same devices. Previously, Chatterjee et. al [7] addressed this problem by developing a transfer function formalism that incorporates plane wave angular spectra of the input beam along with a medium transfer function to derive the output scattered spectra $\tilde{E}_0(\delta)$ and $\tilde{E}_1(\delta)$. This paper extends these efforts by using a simulation to investigate specific limiting behavior of the scattered output in terms of a Gaussian profile input and other system parameters.

An overview of standard AO analysis, called the multiple plane wave scattering technique, which was developed by Korpel and Poon in 1980 [5], is provided in Section 2. This technique describes the interaction of light and acoustic waves, resulting in a set of coupled differential equations. Using the multiple plane wave technique as a starting point, the Bragg diffraction of arbitrary non-uniform input beams using transfer functions is presented in section 3 [7]. This analysis results in expressions for the zero and first orders which are amenable to numerical solution. In section 4, the simulation, based on these expressions, of non-uniform input beams is presented, extending the work reported in [7]. Results for Gaussian inputs are shown and a comparison is made between the numerical results and the known solutions for the plane wave case.

2.　　PRELIMINARY WORK USING MULTIPLE PLANE WAVE SCATTERING TECHNIQUE

By assuming a plane wave input beam, analysis of Bragg diffraction is simplified and both of the output orders are also plane waves. For realistic, non-uniform incident beams, Chatterjee et. al [7] have developed a transfer function approach to describe Bragg diffraction. This technique describes the diffracted orders of light for arbitrary input profiles. The scattered field is represented by a Fourier integral which depends on the input field (angular) spectrum.

When a Bragg cell is incorporated into a feedback circuit, it is possible to create bistability or multistability leading to chaos, which can be exploited for encryption/decryption applications [8, 9]. This is done by using a photo detector to pick up the first order intensity. The output of the photodetector is amplified and used as a bias for the RF generator. A constant offset alpha is added to this bias signal, and this alpha can be used to control the dynamical characteristics.
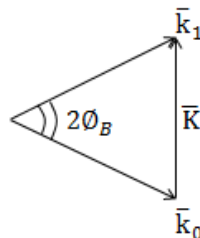

Fig.1: Wavevector diagram for upshifted interaction.

Shown in Fig.1 is a conventional wavevector triad picture indicating pure Bragg diffraction in terms of two photons and one phonon. Thus, $(h/2\pi)\bar{k}_0$, $(h/2\pi)\bar{k}_1$, and $(h/2\pi)\bar{K}$ represent the incident (parallel to the zeroth-order) photon, the first-order (scattered) photon, and the acoustic phonon respectively. Hence, the incident photon in this description *absorbs* a single acoustic phonon to generate a *higher* (first)-order scattered photon of light (thereby generating a positive frequency shift- a fundamental property of acousto-optic up-shifted interactions). We also note that in our multiple plane wave analysis model, the basic interaction is based on the Maxwell's equations and the resulting modulation of the medium refractive index due to the acoustic vibrations in the sound cell. The problem is thereby analyzed using the modified Helmholtz equation in the phasor domain. In view of the above- the photon-phonon

interaction triad discussed above is likely best interpreted as Einstein rather than Planck (or quantum-based) photonic or discrete energy description.

A coupled set of ODEs is used to describe, for an ideal Bragg case in which the input beam is a uniform plane wave, the interaction between light and sound.

$$\frac{dE_1}{d\xi} = -j\frac{\hat{\alpha}}{2}E_0 \quad , \tag{1}$$

$$\frac{dE_0}{d\xi} = -j\frac{\hat{\alpha}}{2}E_1 \quad . \tag{2}$$

In these equations, $\hat{\alpha}$ is the peak phase delay in the medium and $\xi = \frac{z}{L}$ is the normalized propagation distance. These equations, at the output of the Bragg cell ($\xi = 1$), have the solution

$$E_1 = -jE_{inc} \sin\left(\frac{\hat{\alpha}_0}{2}\right) \quad , \tag{3}$$

$$E_0 = E_{inc} \cos\left(\frac{\hat{\alpha}_0}{2}\right) \quad . \tag{4}$$

The intensity signal from the photo detector is therefore $I_1 = I_{inc} \sin^2\left(\frac{\hat{\alpha}}{2}\right)$, where $I_{inc} = |E_{inc}|^2$ [6]. This solution is often used to analyze chaos, but it is limited by the unrealistic assumption of a uniform plane wave input. The motivation of the current work is to explore, using simulations, the behavior of Bragg cells for non-uniform input beams. These results will have implications for feedback behavior.

Strong acoustic-optic interaction was described by Korpel and Poon [5] using a plane wave decomposition with multiple scattering for the interaction. The light and sound fields are represented via plane wave decomposition, and their interaction is described by multiple scattering. This analysis leads to the following set of coupled differential equations for the nth diffracted order [5] in terms of the (n-1) and (n+1) orders under a nearest-neighbor interaction assumption,

$$\frac{d\tilde{E}_n}{d\xi} = -j\left(\frac{\hat{\alpha}}{2}\right)\left[e^{\left\{-j\left(\frac{1}{2}\right)\left[\frac{\phi_{inc}}{\phi_B}+(2n-1)\right]Q\xi\right\}}\tilde{E}_{n-1} + e^{\left\{j\left(\frac{1}{2}\right)\left[\frac{\phi_{inc}}{\phi_B}+(2n+1)\right]Q\xi\right\}}\tilde{E}_{n+1}\right] \quad , \tag{5}$$

with the boundary condition $\tilde{E}_n = \tilde{E}_{inc}\delta_{n0}$ at $z \leq 0$. In these equations, ($\hat{\alpha} = kC|A|L/2$), $\xi = z/L$, and δ_{n0} is the Kronecker delta function [7]. These equations describe the general case, and in order to obtain the two diffracted orders of interest (n=0 and n=1) for Bragg diffraction, set $\phi_{inc} = -(1 + \delta)\phi_B$. In that case, the equations under near-Bragg incidence with an angular deviation $\delta\phi_B$ become:

$$\frac{d\tilde{E}_0}{d\xi} = -j\left(\frac{\hat{\alpha}}{2}\right)e^{-jQ\xi\delta/2}\tilde{E}_1 \quad , \tag{6}$$

$$\frac{d\tilde{E}_1}{d\xi} = -j\left(\frac{\hat{\alpha}}{2}\right)e^{jQ\xi\delta/2}\tilde{E}_0 \quad . \tag{7}$$

When $\delta = 0$, these equations reduced to the usual results (eqs. 1 and 2). The solution of these two equations is used in the transfer function description [1]. The transfer functions $\tilde{H}_0(\delta)$ and $\tilde{H}_1(\delta)$ in the spectral domain are defined as:

$$\tilde{H}_0(\delta) = \frac{\tilde{E}_0(\xi)_{\xi=1}}{\tilde{E}_{inc}} \quad , \tag{8}$$

$$\tilde{H}_1(\delta) = \frac{\tilde{E}_1(\xi)_{\xi=1}}{\tilde{E}_{inc}} \quad . \tag{9}$$

3.   TRANSFER FUNCTION TECHNIQUE FOR ARBITRARY BEAM PROFILES

To study arbitrary input profiles, Chatterjee et. al [7] developed plane wave transfer functions and applied them to two diffracted orders for a Gaussian input beam. Fig. 1 illustrates the geometry for Bragg diffraction with an arbitrary incident beam profile.
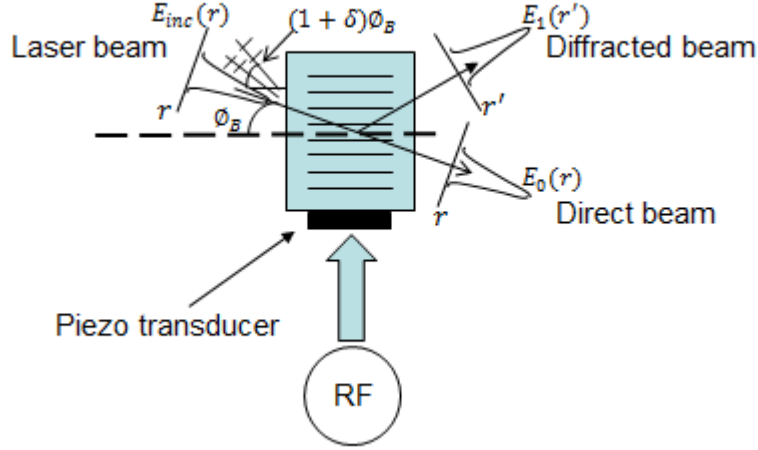

Fig.2: Bragg diffraction with an arbitrary incident beam profile.

The figure assumes upshifted operation at the nominal Bragg angle of incidence. The variable r is the transverse radial coordinate with respect to the direction of the incident field, and r' is similarly defined for the first-order diffracted beam. In order to obtain the scattered fields $E_0(r)$ and $E_1(r')$ from the incident light $E_{inc}(r)$ shown in Fig. 2, a direct Fourier transform approach is used. The transfer functions $H_1(\delta)$ and $H_0(\delta)$ defined in the previous section are used. The output light is generated via inverse Fourier transform [7].

$$E_{out}(r) = \int_{-\infty}^{\infty} \tilde{E}_{inc}(\delta) H(\delta)\, e^{-j\frac{2\pi}{\lambda}\delta\phi_B\, r}\left(\frac{\phi_B}{\lambda}\right) d\delta \,, \tag{10}$$

$$E_{in}(r) = \frac{E_{inc}}{\sigma_1\sqrt{2\pi}}\, e^{-\frac{1}{2}\left(\frac{r^2}{\sigma_1{}^2}\right)}, \tag{10-a}$$

where $\tilde{E}_{inc}(\delta)$ is the angular spectrum of the incident profiled beam [7]. As a particular example, consider a Gaussian input profile. In this case, the inverse Fourier transform becomes:

$$E_0(r) = \int_{-\infty}^{\infty} E_{inc}\, e^{-\frac{1}{2}\left(\frac{\pi\sigma_1}{\Lambda}\right)^2\delta^2}\, e^{-\frac{j\delta Q}{4}} \cdot \left[\cos\left(\sqrt{\left(\frac{\delta Q}{4}\right)^2 + \left(\frac{\hat{\alpha}}{2}\right)^2}\right) + \frac{j\frac{\delta Q}{4}\sin\sqrt{\left(\frac{\delta Q}{4}\right)^2 + \left(\frac{\hat{\alpha}}{2}\right)^2}}{\sqrt{\left(\frac{\delta Q}{4}\right)^2 + \left(\frac{\hat{\alpha}}{2}\right)^2}}\right] \cdot e^{-j2\pi r\left(\frac{\delta}{2\Lambda}\right)}\, d\left(\frac{\delta}{2\Lambda}\right), \tag{11}$$

and

$$E_1(r') = \int_{-\infty}^{\infty} E_{inc}\, e^{-\frac{1}{2}\left(\frac{\pi\sigma_1}{\Lambda}\right)^2\delta^2}\left(\frac{-j\hat{\alpha}}{2}\right) \cdot e^{j\frac{\delta Q}{4}}\frac{\sin\sqrt{\left(\frac{\delta Q}{4}\right)^2 + \left(\frac{\hat{\alpha}}{2}\right)^2}}{\sqrt{\left(\frac{\delta Q}{4}\right)^2 + \left(\frac{\hat{\alpha}}{2}\right)^2}} \cdot e^{+j2\pi r'\left(\frac{\delta}{2\Lambda}\right)}\, d\left(\frac{\delta}{2\Lambda}\right). \tag{12}$$

In these equations, σ_1 represents the standard deviation of the input Gaussian beam. In the following section, the simulation is used to produce scattered and undiffracted outputs consistent with these equations, and the results are discussed.

4. SIMULATION RESULTS

The motivation for this current work is to simulate and further explore Gaussian input beams since real laser beams are profiled and commonly Gaussian. Most researchers assume a uniform plane wave input profile to simplify the analysis, and the effects of non-uniform profiles are not well studied. The simulation described in this work implements the transfer function formalism for an arbitrary Gaussian input profile as described by eqs. (11) and (12). This simulation is consistent with the limiting cases but offers results for more realistic scenarios that cannot be obtained with the uniform plane wave assumptions. After describing these new results, their implications for AO hybrid feedback systems are discussed.

Figs. 3-5 illustrate the scattered first-order beam output $|E_1(r', \hat{\alpha}))|$ from different perspectives for Q=20. For this relatively low Q, these results seem to maintain the expected (*uniform* plane wave) behavior. Fig. 4 illustrates the output cross sections of first order diffraction for a Gaussian input profile for Q=20. Note that the 2-D profile has a $\sin^2$-type appearance. However, this may not be exactly so, as we later find from feedback simulations.   Fig. 5 shows that the cross section along the other dimension is approximately Gaussian.
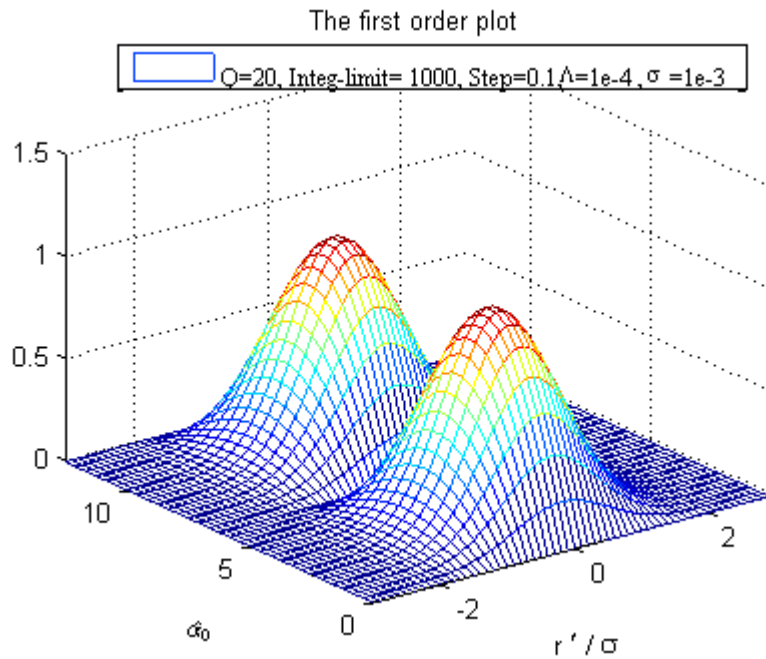

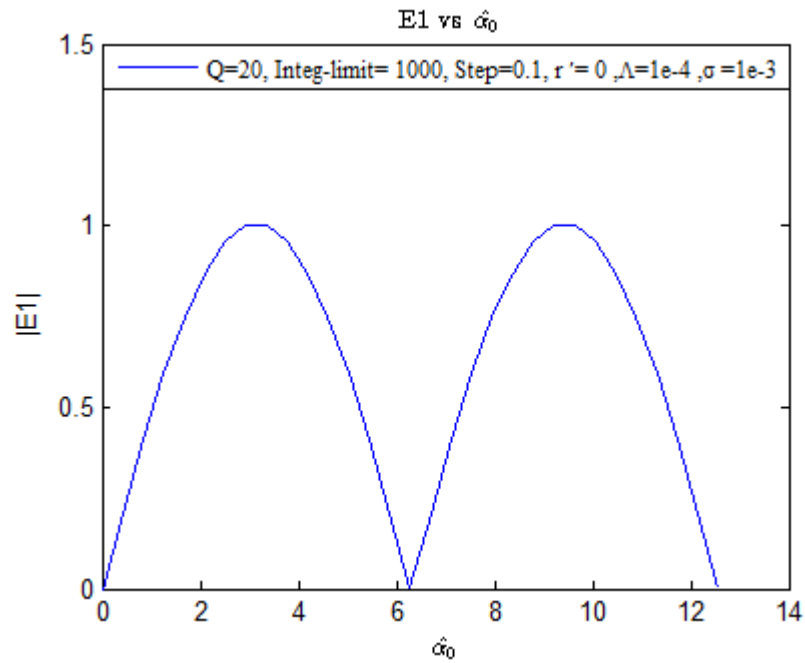Fig.3. Bragg diffraction with an arbitrary incident beam profile for Q=20.

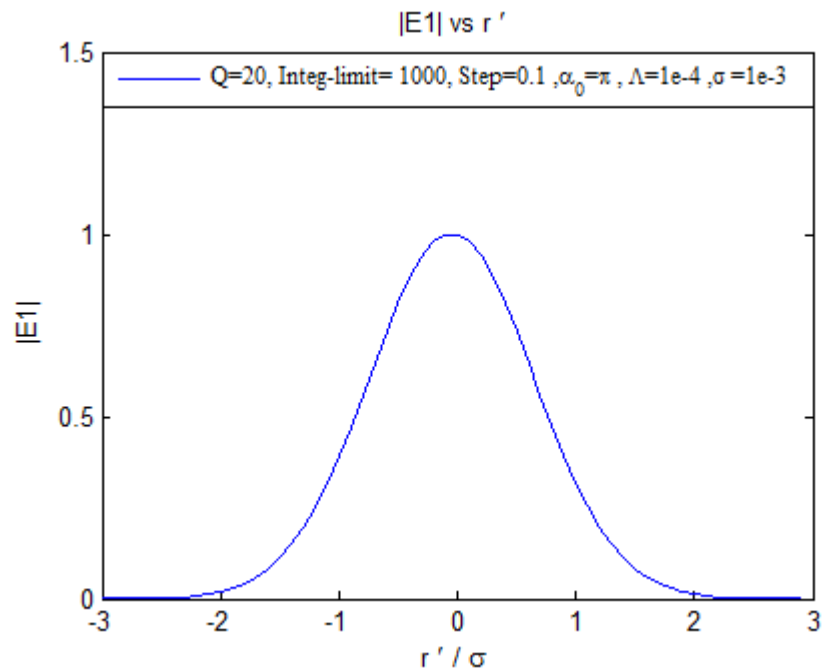Fig.4. First-order Bragg diffraction versus the optical phase shift (cross section from Fig.3).

Fig.5. First-order Bragg diffraction versus the normalized transverse radial coordinate (cross section from Fig.3).

At higher values of Q, the output is no longer Gaussian. Figs. 6-8 illustrate the scattered first-order beam output $|E_1(r', \hat{\alpha}))|$ from different perspectives for Q=177. Fig.6 shows the behavior in 3D. At this Q value the profile shape deviates from the expected behavior. Fig. 7 illustrates the output cross sections of first-order diffraction for a Gaussian

input profile for Q=177. Fig. 8 shows the cross section along the normalized transverse radial coordinate for $\hat{\alpha}_0 = \pi$, and is seen to be no longer Gaussian. We also note that the $\hat{\alpha}_0$ - profile is clearly different from the ideal $\sin^2$ behavior.
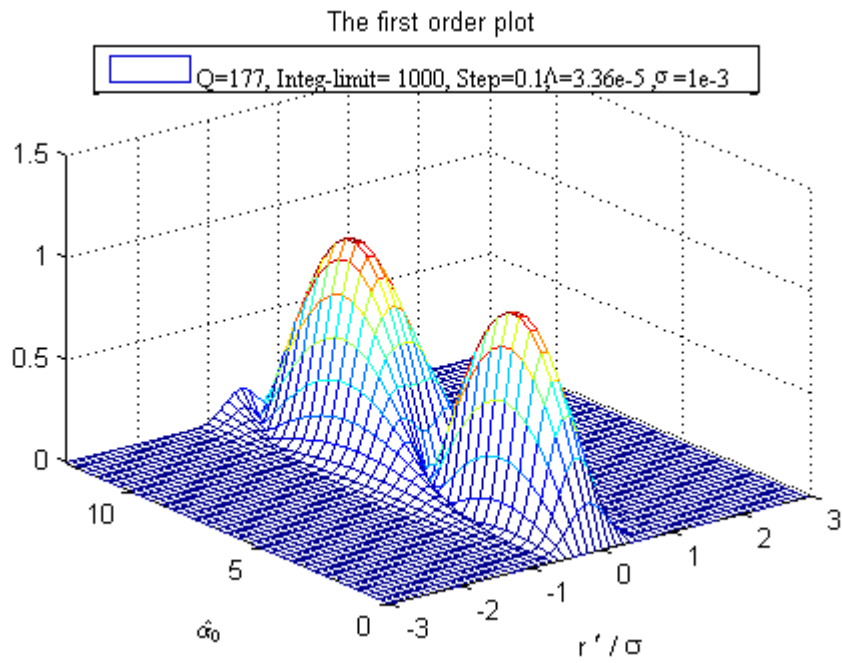

Fig.6. Bragg diffraction with an arbitrary incident beam profile for Q=177.
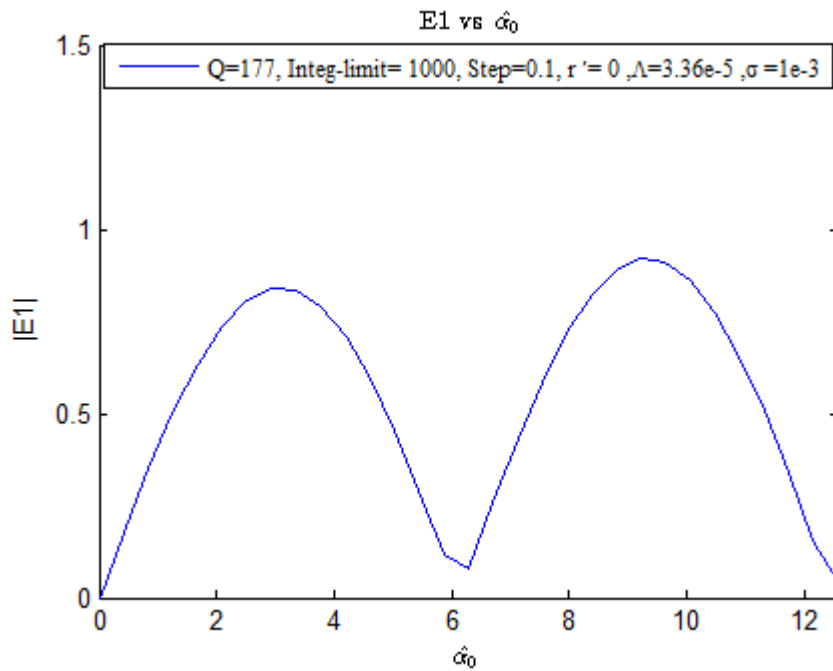

Fig.7. First-order Bragg diffraction versus the optical phase shift (cross section from Fig.6).
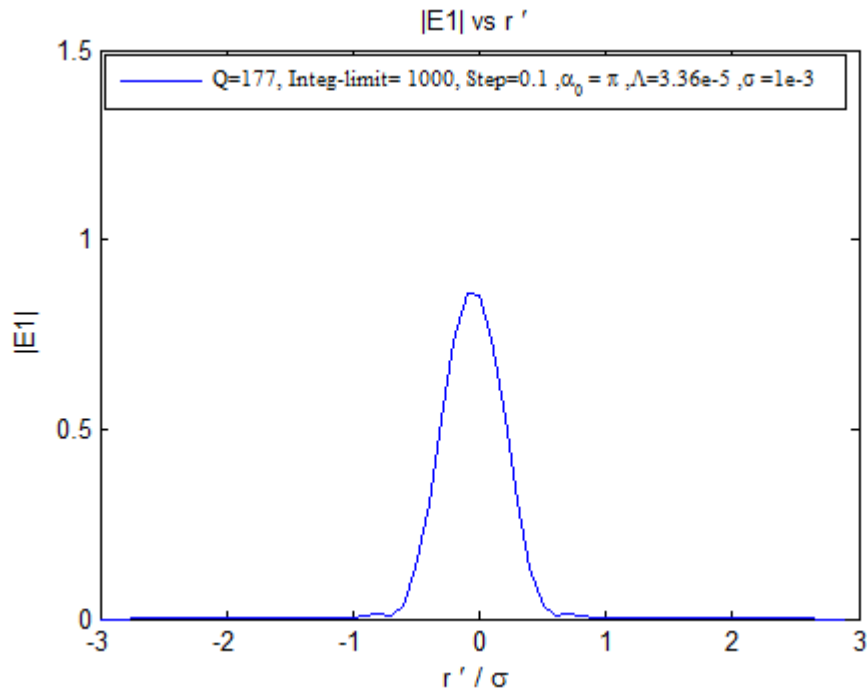
Fig.8. First-order Bragg diffraction versus the normalized transverse radial coordinate (cross section from Fig.6).

Figs. 9-11 illustrate the scattered first-order beam output $|E_1(r', \hat{\alpha}))|$ from different perspectives for Q=533. At this Q value the profile shape is further deviated from the expected behavior. Fig. 9 shows the behavior in 3D. Fig. 10 illustrates the output cross sections of first order diffraction for a Gaussian input profile for Q=533 which is even more deviated from the $\sin^2$ profile. Fig. 11 shows that the cross section along the normalized transverse radial coordinate for $\hat{\alpha}_0 = \pi$ is clearly no longer Gaussian.
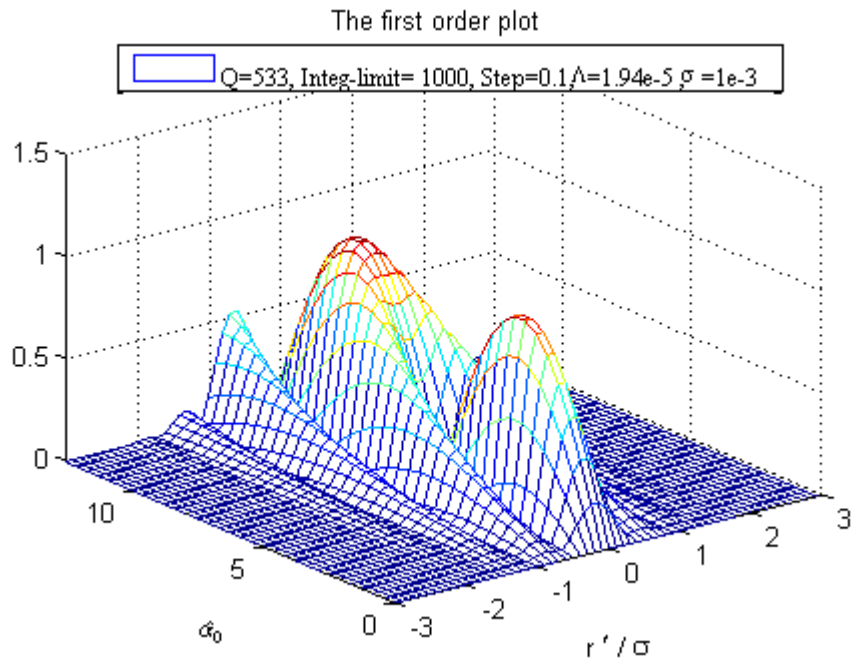

Fig.9. Bragg diffraction with an arbitrary incident beam profile for Q=533.

E1 vs $\hat{\alpha}_0$

Fig.10. First-order Bragg diffraction versus the optical phase shift (cross section from Fig.9).
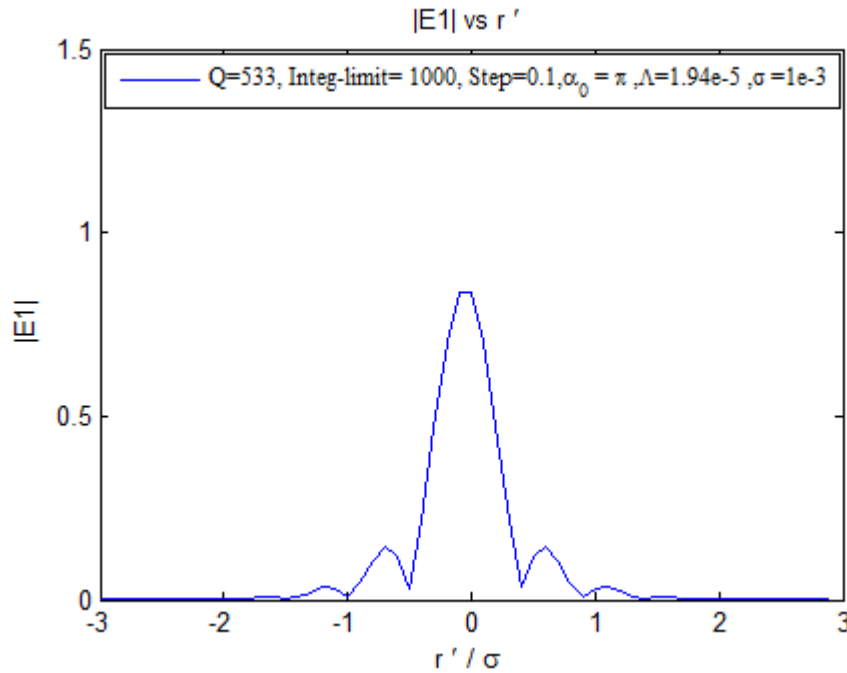
|E1| vs r′

Fig.11. First-order Bragg diffraction versus the normalized transverse radial coordinate (cross section from Fig.9).

The simulation was used predict the output for a uniform plane wave by choosing a very wide Gaussian input. In this case for Q=20, shown in Fig. 12, the output along the $\hat{\alpha}_0$ dimension resembles a $\sin^2$ function, which is consistent with the literature. Also, the output is nearly uniform along the other dimension, indicating uniform profile behavior.
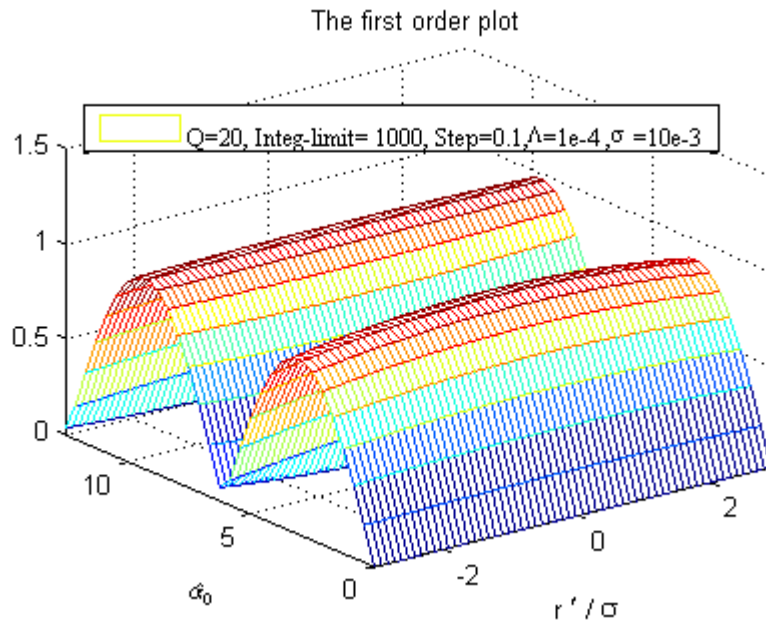
The first order plot

Q=20, Integ-limit= 1000, Step=0.1,Λ=1e-4,σ =10e-3

$\hat{\alpha}_0$

r'/σ

Fig.12: First-order Bragg diffraction with a wide incident beam.

E1 vs $\hat{\alpha}_0$

Q=20, Integ-limit= 1000, Step=0.1, r '= 0 ,Λ=1e-4 ,σ =10e-3
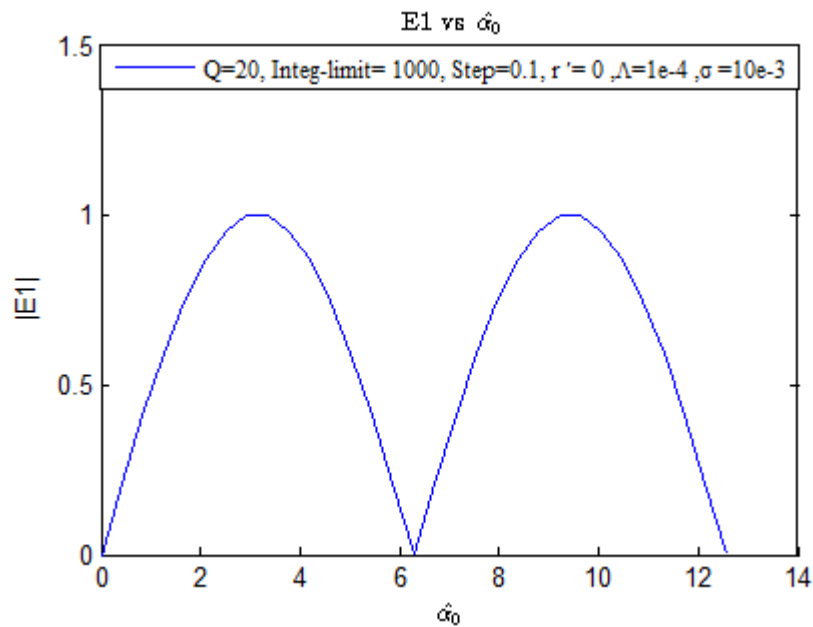
|E1|

$\hat{\alpha}_0$

Fig.13. First-order Bragg diffraction versus the optical phase shift (cross section from Fig.12).

Fig. 13 illustrates the output cross sections of first order diffraction for a uniform plane wave for Q=20. Fig. 14 shows that the cross section along the normalized transverse radial coordinate for $\hat{\alpha}_0 = \pi$ is nearly uniform.
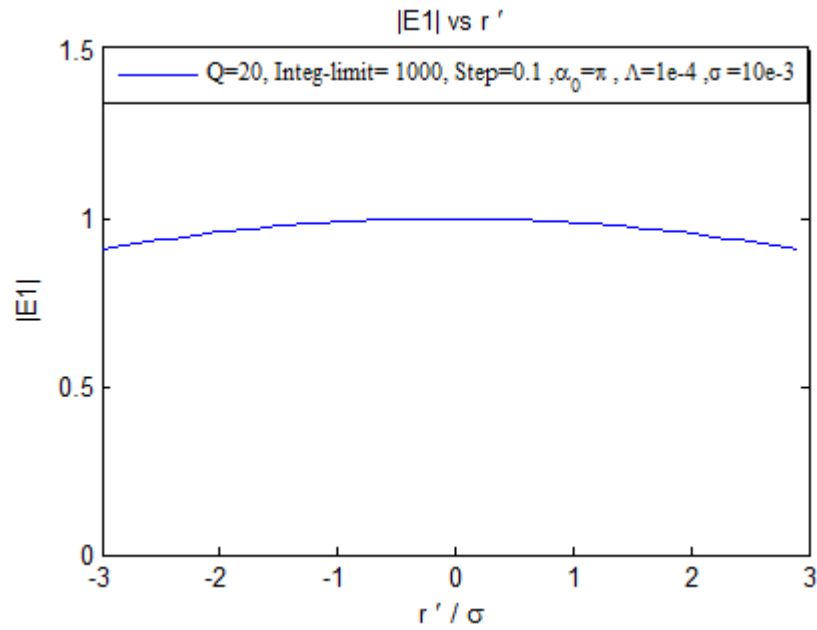
Fig.14. First-order Bragg diffraction versus the normalized transverse radial coordinate (cross section from Fig.12).

The theory in [7] predicts a spatial shift in the output profile for large values of $\hat{\alpha}$; however, for all the cases shown previously, the shift is negligible. According to [7], as $\hat{\alpha}_0$ goes to infinity, the shift off center approaches $-Q\Lambda/4\pi$. Fig. 15 displays the simulation results for $\hat{\alpha}_0 = 20\pi$ and the contour lines clearly illustrate the shift.
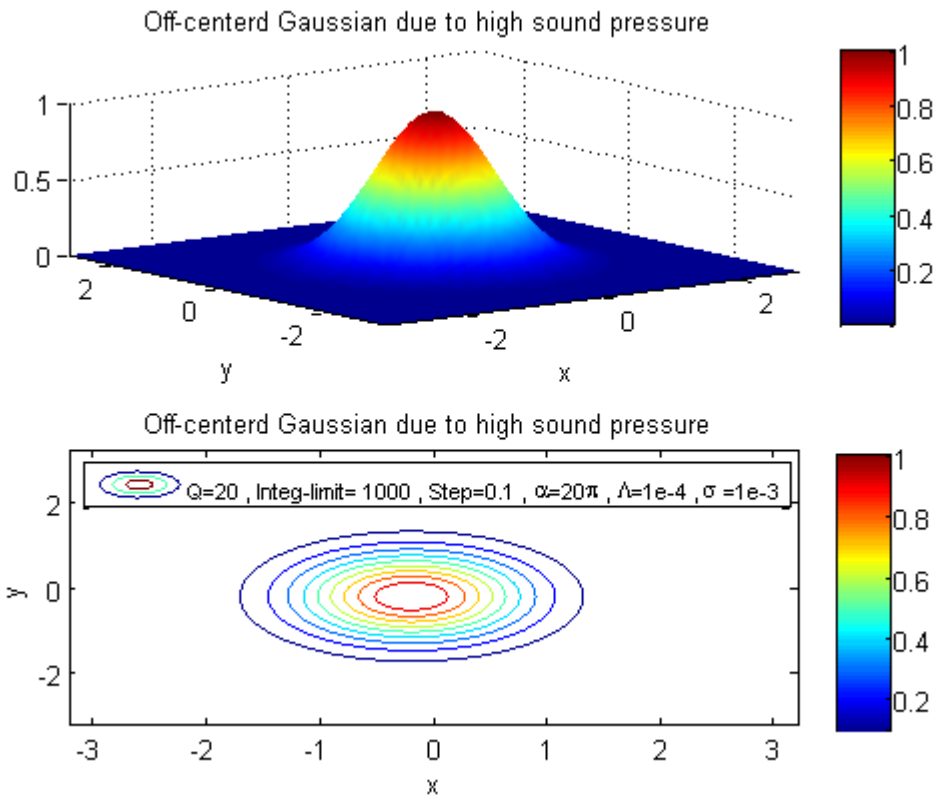

Fig.15. The asymptotic axial shift of the beam center as predicted by the transfer function formalism.

5.　CONCLUDING REMARKS AND FUTURE WORK

Recent results from an AO Bragg cell under first-order intensity feedback, while satisfactory, are limited notionally by the standard AO assumption of *uniform* plane waves of light and sound.　Nominally, for uniform plane waves, the Bragg-diffracted first-order light is a $\sin^2$ function versus the optical phase-shift parameter ($\hat{\alpha}_0$).　An earlier model developed for Gaussian *profiled* plane waves predicted approximately Gaussian scattered beams distorted at higher Q (Klein-Cook) values.　We presented here *profiled* optical plane wave propagation through a Bragg cell, examining the scattered first-order beam from different perspectives. First, it is found that for profiled beams, the first-order light does not display the $\sin^2$ characteristic that occurs in the uniform plane wave case. Second, at higher Q-values the output begins to distort along both dimensions.　This is particularly counter-intuitive, since at higher Q, one would expect the device to behave more Bragg-like than at lower Qs.　This may have implications embedded in the properties of photon scattering by phonons, and might well be an area worthy of further explorations.　A third observation in the asymptotic limit $\hat{\alpha}_0 \to \infty$ shows an axial shift of the beam profile in the first order, conforming to wave theory predictions; however, the shift appears to exist only on one side of the radial axis (3rd quadrant in the XY plane) and not the others. This finding is also open to explanations based on possible photon scattering by a Bragg cell under profiled beam diffraction.

REFERENCES

1.　A. Korpel, "Acousto-Optics," 2nd edition (Marcel Dekker, New York, 1997).

2.　W.R. Klein and B.D. Cook, "Unified approach to ultrasonic light diffraction," IEEE Trans. Sonics Ultrason. SU-14, 123–133 (1967).

3.　S.-T. Chen, and M. R. Chatterjee "A numerical analysis and expository interpretation of the diffraction of light by ultrasonic waves in the Bragg and Raman-Nath regimes multiple scattering theory," IEEE Trans. on Education, 39, issue 1, 56-68 (1996).

4.　C. Webb, and J. Jones, "Handbook of laser technology and applications - Vol. II," 1st edition (IOP, Cornwall, UK, 2004).

5.　A. Korpel and T.-C. Poon, "Explicit formalism for acousto-optic multiple plane-wave scattering," J. Opt. Soc. Am., 70, 817–820 (1980).

6.　M.R. Chatterjee and J.-J. Huang, "Demonstration of acousto–optic bistability and chaos by direct nonlinear circuit modeling," Appl. Opt. 31, 2506-2517 (1992).

7.　M.R. Chatterjee, T.-C. Poon, and D.N. Sitter, Jr., "Transfer function formalism for strong acousto-optic Bragg diffraction of light beams with arbitrary profiles," Acustica 71 [1990], 81-91.

8.　J. Chrostowski and C. Delisle, "Bistable piezoelectric Fabry–Perot interferometer" Can. J. Phys., 57, 1376-1379 (1979).

9.　J. Chrostowski and C. Delisle, "Bistable optical switching based on Bragg diffraction," Opt. Commun. 41, 71–74 (1982).